Abbreviation and Acronym
PTFE = polytetrafluoroethylene

difficult exposure, the fourth costal bone was cut to make a larger working space. This bone was repaired with a hydroxyapatite-poly-L-lactide plate (Osteotrans MX; Takiron Co Ltd, Osaka, Japan) at the end of the surgery, and pseudoarthrosis at the rib-costal cartilage was prevented.[5] Cardiopulmonary bypass was established with the femoral artery (16F–20F FEM-Flex II arterial cannula; Edwards Lifesciences, Irvine, Calif), femoral vein (20F–24F VFEM venous cannula, Edwards Lifesciences), and right jugular vein (16F FEM-Flex II arterial cannula, Edwards Lifesciences) cannulation under transesophageal echocardiography guidance. The heart was arrested with antegrade cold blood cardioplegia infusion through a root cannula under direct crossclamping of the ascending aorta with a modified Cosgrove flexible clamp. Infusion of the cardioplegia was repeated every 30 minutes with topical cooling. The mitral valve was exposed thorough the interatrial grove approach with a left atrial retractor attached to a minithoracotomy spreader and an additional retractor for the posterior wall of the left atrium attached to the spreader. Multiple chordal reconstructions by the loop technique[6,7] with PTFE Gore-Tex CV-5 sutures were applied for correction of prolapsed leaflet rather than the resection and suture technique since 2005.[8] We routinely prepare the PTFE loops in the same length in almost all cases and adjust the efficient length of the neochordae with the secondary loop for the mitral leaflet depending on the size of the left ventricle and the part of the prolapsed leaflet (loop-in-loop technique). A reusable clip as a substitution for the neurosurgery clip was used to tie the PTFE suture firmly in the correct position without slipping. A flexible silicon ring sizer was used to choose the annuloplasty ring size so it can pass easily thorough a narrow working port without tissue damage. All manipulations in the heart were performed under endoscope assistance. However, surgeons did not always use endoscopic vision and used direct vision when they were comfortable with it.

RESULTS

No operative mortality after the surgery occurred (Table 1). There were 2 intraoperative conversions to median sternotomy for correction of retrograde aortic dissection (1) and for coronary artery bypass grafting to the left anterior descending artery area (1). There were 2 early reoperations for mitral valve repair failure and 3 reoperations for bleeding. No severe cerebral complication occurred. Since the new retractor was launched in 2010, there has been no conversion to median sternotomy and reoperation for bleeding among 53 cases. The mean aortic crossclamp time was 163.8 ± 42.0 minutes. Annuloplasty with ring or band was done in all but 1 case. The loop technique was used in 173 cases (68.6%). Among them, a combination of the loop-technique and resection-and-suture technique was used in 56 cases with complicated mitral valve pathology. After 2010, the loop technique was used in 47 cases (88.7%).

TABLE 1. Surgical outcome between 1998 and April 2011 (n = 252)

Age, y	51.1 ± 13.9
Male/female	159/93
Operative mortality	0
Conversion to sternotomy	2
Early reintervention	
Failure of mitral valve repair	2
Surgical bleeding	3
Aortic crossclamp time	163 ± 42.0
Loop technique	173 (68.6%)
After 2010	47/53 (88.7%)
Loop technique+resection and suture	56 (22.2%)

DISCUSSION

The newly developed left atrial retractor system, including a minithoracotomy spreader, a left atrial blade, and an additional retractor for the posterior wall of the left atrium, is specialized for mini-mitral surgery and can solve all kinds of difficulties in exposure of the mitral valve. The advantage of this mini-valve system is the flexibility. It moves flexibly to various positions and has good positioning of retractors for optimum exposure depending on the situation and the surgeon's choice. A 5 blade size is available depending on the left atrial size and target legion. To adapt the size of the blade to the pathologic legion, the left atrial retractor can be exchanged easily to the other size under fixed optimal exposure. By retraction of the anterior mitral leaflet toward the anterior wall of the left ventricle with the smallest size blade deeply inserted, even papillary muscles can be exposed easily and clearly on the straight view through the small working port. This function enables comfortable manipulation to the papillary muscle in chordal reconstruction with the loop technique. The exposure of the P2 to P3 area of the mitral valve usually is difficult because of elevation of the left atrial wall. To solve this problem, an additional retractor attachable to the minithoracotomy retractor can push the left atrial wall away from the surgeon's sight. In case of unfavorable exposure of the P1 area, the additional retractor can be used alternatively for retraction of the anterolateral side of the left atrial wall.

Correct sizing of the annuloplasty ring is an important and critical part of the mitral valve repair but is difficult through a small working port. A homemade flexible silicon ring sizer was developed as the same size as the official sizer of the Physio II mitral annuloplasty ring (Edwards Life Science). This can easily pass thorough a narrow working port without tissue damage and is helpful for correct sizing under endoscopic vision.

To repair a prolapsed leaflet in the mitral valve, the gold standard has been the resection-and-suture technique of the prolapsed leaflet, which has demonstrated excellent long-term results.[9] In contrast, the "respect rather than resect" approach proposed by Perier and colleagues,[10] which respects leaflet tissue as an important component of the coaptation surface and preserves leaflet without resection, is widely accepted because it allows a larger coaptation area than the resection-and-suture technique and has an advantage in dynamic distribution of forces and stress on valve components and the left ventricle. Especially in cases

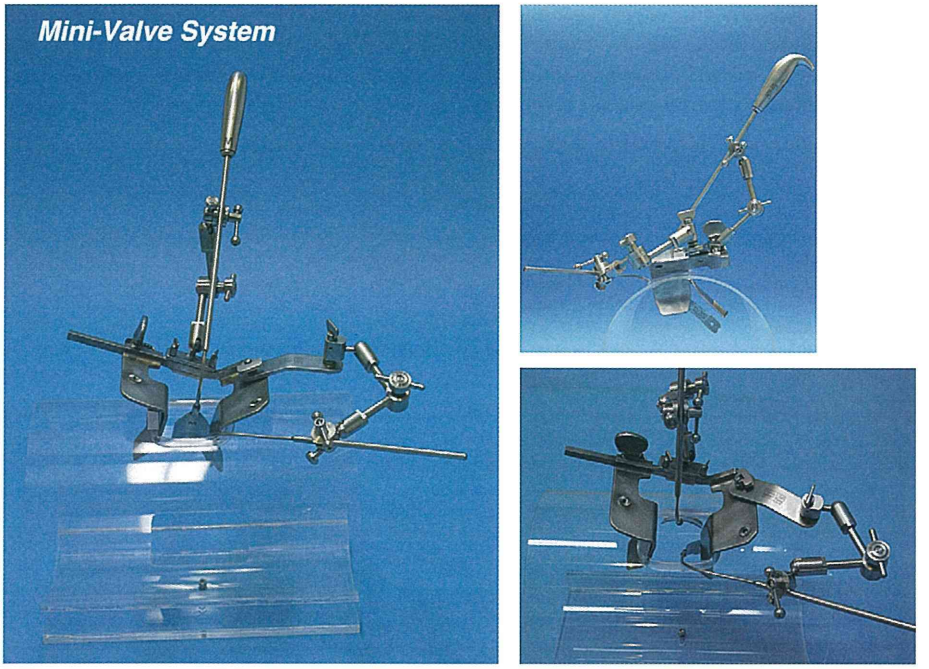

FIGURE 1. Mini-valve system is composed of a mini-thoracotomy spreader with a tilted blade, a left atrial retractor that moves flexibly, and an additional blade for the posterolateral wall of the left atrium.

with broad prolapse of the posterior leaflet or with anterior leaflet prolapse, multiple chordae reconstruction using PTFE suture is essential. The loop technique is a modification that normally uses 4 premade PTFE loops to facilitate chordal reconstruction. In mini-mitral surgery with a limited working area, multiple chordal reconstructions with individual PTFE sutures are technically difficult and even dangerous because of the risk of injury in the papillary muscle. The loop technique is a feasible solution to preserve as much leaflet area as possible and to repair the broad prolapsed leaflet in mini-mitral surgery. The loop-in-loop technique avoids the surgical manipulation in the deep working area at the base of the left ventricle and facilitates multiple reconstructions of neochordae. The technique also enables reattachment of the neochordae when residual leakage is found in the saline injection test. Recently, 88.7% of mitral valve repairs were done with the loop technique, and the variation of the repair method is increasing to treat various type of mitral valve pathology.

For all these advantages in the loop technique, many surgeons still hesitate to adapt this technique because surgeons feel uncomfortable when they tie slippery PTFE (Gore-Tex) sutures many times. To solve this problem and help surgeons tie many knots with PTFE suture in the correct position, a reusable clip as a substitution for the neurosurgery clip is used to tie the PTFE suture firmly without slipping. The length of the second loop to fix the premade loops with PTFE suture is determined after filling the left ventricle with saline and appropriately positioning the clip, which can easily slide to the best position when the leakage disappears.

Although this study shows longer mean aortic cross-clamp times than a previous study on mitral valve repair, the surgical outcome is excellent with no surgical mortality. This is supported by careful myocardial protection with antegrade cold-blood cardioplegia infusion under transesophageal echocardiography monitoring of the aortic valve and aortic root pressure during infusion. During cardioplegia, surgeons and anesthesiologists should ensure the aortic valve is incompetent, the cardioplegic solution is running into the coronary artery, and the aortic root pressure is sufficiently high. To afford an incompetent aortic valve, the left atrial retractor should be released during cardioplegia. The mini-valve system can aid in easy release and repositioning of the left atrial retractor after repeated cardioplegic shots. This secure strategy in myocardial protection may help beginner surgeons using the mini-mitral approach to achieve good results in cases of complex mitral valve pathology.

CONCLUSIONS

In an optimal operative setting, mitral valve repair via minithoracotomy is a feasible and durable procedure with minimal mortality and morbidity. The feasibility of multiple PTFE chordae reconstructions is an important strategy especially when trying to preserve leaflets. To reconstruct multiple chordae with PTFE suture, the loop technique is essential in mitral valve repair via minithoracotomy. New

innovative instruments and a refined surgical setting in mini-valve surgery facilitate both direct-vision and endoscopic-assisted approaches even in complex pathology and contribute to the acceptance of mini-mitral valve surgery as a routine surgery.

References

1. Casselman FP, Van Slycke S, Wellens F, De Geest R, Degrieck I, Van Praet F, et al. Mitral valve surgery can now routinely be performed endoscopically. *Circulation*. 2003;108(Suppl 1):II48-54.
2. Modi P, Rodriguez E, Hargrove WC 3rd, Hassan A, Szeto WY, Chitwood WR Jr. Minimally invasive video-assisted mitral valve surgery: a 12-year, 2-center experience in 1178 patients. *J Thorac Cardiovasc Surg*. 2009;137:1481-7.
3. Seeburger J, Borger MA, Falk V, Kuntze T, Czesla M, Walther T, et al. Minimal invasive mitral valve repair for mitral regurgitation: results of 1339 consecutive patients. *Eur J Cardiothorac Surg*. 2008;34:760-5.
4. Gammie JS, Zhao Y, Peterson ED, O'Brien SM, Rankin JS, Griffith BPJ. Maxwell Chamberlain Memorial Paper for adult cardiac surgery. Less-invasive mitral valve operations: trends and outcomes from the Society of Thoracic Surgeons Adult Cardiac Surgery Database. *Ann Thorac Surg*. 2010;90:1401-8. 10 e1; discussion 8-10.
5. Ito T, Kudo M, Yozu R. Usefulness of osteosynthesis device made of hydroxyapatite-poly-L-lactide composites in port-access cardiac surgery. *Ann Thorac Surg*. 2008;86:1905-8.
6. Falk V, Seeburger J, Czesla M, Borger MA, Willige J, Kuntze T, et al. How does the use of polytetrafluoroethylene neochordae for posterior mitral valve prolapse (loop technique) compare with leaflet resection? A prospective randomized trial. *J Thorac Cardiovasc Surg*. 2008;136:1206.
7. Kuntze T, Borger MA, Falk V, Seeburger J, Girdauskas E, Doll N, et al. Early and mid-term results of mitral valve repair using premeasured Gore-Tex loops ('loop technique'). *Eur J Cardiothorac Surg*. 2008;33:566-72.
8. Kudo M, Yozu R, Kokaji K, Kimura N, Kobayashi M, Takahashi T. Examination of mitral valve repair with port-access method: aiming at early and less invasive mitral valve repair. *Gen Thorac Cardiovasc Surg*. 2009;57:298-302.
9. Perier P, Stumpf J, Gotz C, Lakew F, Schneider A, Clausnizer B, et al. Valve repair for mitral regurgitation caused by isolated prolapse of the posterior leaflet. *Ann Thorac Surg*. 1997;64:445-50.
10. Perier P, Hohenberger W, Lakew F, Batz G, Urbanski P, Zacher M, et al. Toward a new paradigm for the reconstruction of posterior leaflet prolapse: midterm results of the "respect rather than resect" approach. *Ann Thorac Surg*. 2008;86:718-25.

000 New innovative instruments facilitate both direct-vision and endoscopic-assisted mini-mitral valve surgery

Ryohei Yozu, MD, PhD, Kazuma Okamoto, MD, PhD, Mikihiko Kudo, MD, PhD, Hidenori Nonaka, BE, and David H. Adams, MD, Tokyo, Japan and New York, NY

Newly innovated mini-valve systems, including a mini-thoracotomy spreader and left atrial retractors, and specific surgical techniques designed for working in a limited space facilitate mitral valve surgery via mini-thoracotomy. The special setting realizes a favorable surgical outcome even in the complex pathology of mitral valve insufficiency.

心臓手術の実際 第19回

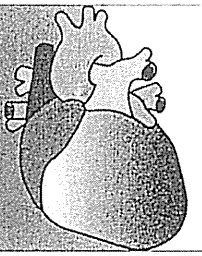

外科医が語る術式，
麻酔科医が語る心臓麻酔，
臨床工学技士が語る体外循環法

監　修
許　俊鋭（東京大学医学部重症心不全治療開発講座）
山田芳嗣（東京大学大学院医学系研究科外科学専攻 生体管理医学講座麻酔学）

協力監修
林田眞和（順天堂大学医学部附属順天堂医院麻酔科・ペインクリニック，同大学大学院疼痛管理学（麻酔科・ペインクリニック講座））
西部伸一（埼玉医科大学国際医療センター麻酔科）
百瀬直樹（自治医科大学附属さいたま医療センター臨床工学部）

低侵襲心臓外科手術（MICS）における体外循環法

―慶應義塾大学病院―

ここでは，低侵襲心臓外科手術（MICS）における僧帽弁手術について解説する．当院では，1998年よりMICSを開始し，550例以上の症例に対し行ってきた．MICSにおいては確実な体外循環の確立，視野展開が何よりも重要であり，そのためには臨床工学技士，麻酔科医との連携が重要である．

外科医
慶應義塾大学医学部外科（心臓血管）
根本　淳 *NEMOTO, Atsushi*
四津良平 *YOZU, Ryohei*

麻酔科医
慶應義塾大学医学部麻酔学教室
山田達也 *YAMADA, Tatsuya*

臨床工学技士
慶應義塾大学病院医用工学センター
又吉　徹 *MATAYOSHI, Toru*

外科医　麻酔科医　臨床工学技士

低侵襲心臓外科手術（MICS）における僧帽弁手術

1 低侵襲僧帽弁手術について

リウマチ熱の減少により僧帽弁狭窄症（mitral stenosis：MS）の発症頻度が低下している一方で，感染や変性疾患を主体とした僧帽弁閉鎖不全の症例は増加の一途をたどっている．

MSでは，左房からの血液の流出が妨げられるために房室間に圧差を生じ，血流の維持のために左房圧が上昇する．さらに上昇した左房圧が肺循環に伝わり，肺高血圧を呈する．そのため肺の間質に体液貯留を生じ，心不全症状を生じる．僧帽弁閉鎖不全では，左室の血液の一部が左房に駆出される．そのため，左房の拡大，左房圧の上昇，大動脈へ向かう拍出量の低下，拡張期に左房へ逆流した血流が左室へ戻ることによる左室の容量負荷を生じる．急性僧帽弁閉鎖不全では左房圧の上昇による肺水腫様の症状を呈し，慢性僧帽弁閉鎖不全では左房拡大が徐々に進行して左室の容量負荷が増大し，左心室の収縮能低下による低心拍出症状，心不全症状を呈する．

現在，僧帽弁閉鎖不全の症例においてはほとんどの症例で僧帽弁形成術（mitral valve plasty：MVP）が可能となりつつあり，僧帽弁閉鎖不全に対する治療戦略が，心不全既往のない症例や心房細動発症前・左心房拡大前というように，より早期での手術に移行する傾向にある．今後はMVPの治療成績はもとより，手術の低侵襲化という概念も重要である．1997年にChitwoodらは，従来のstandard MICS（minimally invasive cardiac surgery）よりさ

らに低侵襲化を目指したまったく胸骨の切開を行わないport-accessの手法を取り入れた，右第4肋間開胸での内視鏡下MVPを報告した[1]．当院でも1998年よりMICSを開始し，現在までに550例以上の症例に対し行ってきた．特に心房中隔欠損症，僧帽弁疾患に関してはMICSを第一選択としており，本稿では，MICSにおける僧帽弁手術について解説する．

2 当院における低侵襲僧帽弁手術の実際

2-1 皮膚切開から体外循環確立まで

体位は仰臥位，軽度右前斜位とし，麻酔は通常の気管挿管を行う．分離肺換気用のユニベントチューブを挿入している．右内頸静脈より「プリセップCVオキシメトリーカテーテル®」(エドワーズライフサイエンス(株))，脱血カニューレ挿入用に5 Frの「シースイントロデューサー」(東レ・メディカル(株))を挿入している．通常，皮膚切開は右乳腺下第4肋間で約5 cmの切開を行うが，女性患者では右乳房下縁を切開線とし，乳腺組織を上方に展開した後に第4肋間で開胸している[2]．片肺換気下に肋間開胸後，肺をよけ心臓の位置を心膜切開前に確認し，視野が狭すぎるようであれば上下どちらかの肋骨を肋軟骨部分で離断して視野を展開する．

体外循環は大腿動静脈からの経皮的心肺補助循環(percutaneous cardiopulmonary support：PCPS)用のカニューレ，および右内頸静脈からの脱血カニューレで確立する．送脱血カニューレ挿入はそれぞれ経食道心エコー(transesophageal echocardiography：TEE)モニタ下に確実に行っている．体外循環開始後，軽度脱血した部分体外循環下の状態で心膜を切開し，心膜および横隔膜を経皮的に牽引し皮膚に固定する(endoclose technique)ことで，視野およびworking spaceの展開を行う．脱血方法は陰圧吸引補助脱血法を採用しており，以前は1本の脱血カニューレのみで行っていたが，現在は右内頸静脈からの脱血カニューレを追加しており，上下大静脈のテーピングなしでも，左心房に肺静脈からの還流が多すぎて視野展開に難渋することはなく，良好な術野が得られる．

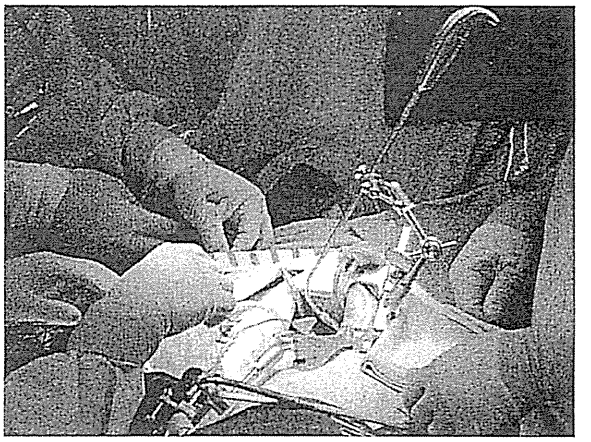

図1 「Adams-Yozu Mini-Valve System®」(UNIMEDIC Ltd.)

大動脈遮断鉗子としては，操作性の良さと簡便性を鑑み，「Cosgrove Flex Clamp®」(エドワーズライフサイエンス(株))を第一選択とし，どうしても視野の邪魔になりそうな場合などは「Modified Cosgrove Flex Clamp®」を術野以外の肋間から用いることとしている．

2-2 僧帽弁の展開

良好な視野展開は弁形成を成功させるための必要条件であり，特に左房・左室の無血視野が大切なことはいうまでもない．そこで，なるべく僧帽弁を正面視するために，僧帽弁への到達法は右側左房切開を原則にしている．左房切開の後に，自作のatrialリトラクター(鈎)を中隔にかけて上方に牽引し，僧帽弁を展開する．このリトラクターの把持には，以前はAESCULAP Inc.のエアサスペンション式のユニトラック・リトラクションシステムを用いていた．現在は我々がUNIMEDIC Ltd.と開発した「Adams-Yozu Mini-Valve System®」を用いている．このシステムの利点は，術野露出のためにさまざまな位置にリトラクターを把持することが可能であり，以前のものよりコンパクトな設計であるため術者，助手の心内操作を妨げずに術野を維持可能な点である[3](図1)．

右前胸部(第4肋間)の小切開は，深い術野

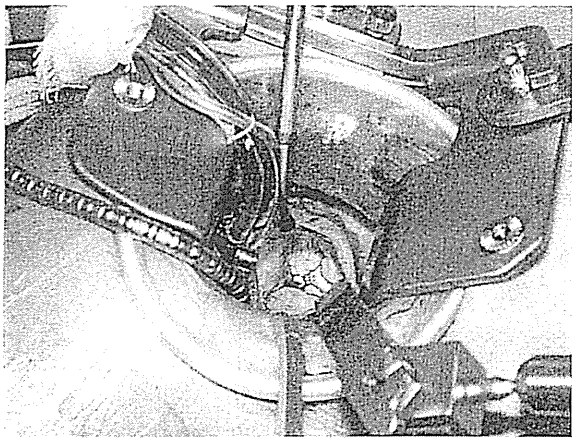

図2　術者からの視野

ではあるが，通常の胸骨正中切開より僧帽弁を正面視することが可能である．また，左房後壁・側壁の牽引には開胸器に固定して把持できるセルフリトラクターシステムを開発し，さらなる良好な視野と working space の確保が可能となっている（図2）．MICS における MVP では MICS 用の特別な機械を用いるが，僧帽弁形成法自体は通常の場合と同様である．

3 臨床工学技士が知っておくべき低侵襲僧帽弁手術に関連した周辺知識

3-1　確実な体外循環確立

体外循環は大腿動静脈，および右内頸静脈から挿入した PCPS 用のカニューレで確立するが，MICS の場合，安全・確実な体外循環の確立は非常に重要である．大腿動静脈よりのカニューレはカットダウンにて挿入しており，そのサイズは臨床工学技士と相談して決定している．大腿動脈の径が細い場合は，両側の大腿動脈から送血している．

送脱血カニューレ挿入時には，TEE にて先行させたガイドワイヤの位置が胸部下行大動脈内および右心房内にあることを確実に確認し，さらに大腿静脈から右心房内まで挿入する脱血カニューレは，ガイドワイヤを通して確実に右心房内に挿入されていることを TEE で確認している．MICS でこのような安全な体外循環確立を確実にするには，麻酔科医の協力が不可欠である．当院では，MICS に際しては，日本周術期経食道心エコー認定（Japanese Board of Perioperative Transesophageal Echocardiography：JB-POT）の資格をもつ麻酔科医が必ず立ち会うこととしている．そのため，手術中には麻酔科医から TEE を通しての多岐にわたる情報がリアルタイムにもたらされ，たいへん有用である．

3-2　大動脈遮断法・心停止・確実な心筋保護

大動脈遮断直後に大動脈基部に刺入したルートカニューレより心筋保護液を注入し心停止を行う．この場合の注意点は，何らかの理由で大動脈弁閉鎖不全の状態を発症し心筋保護液が左室に流れ込むことがあるため，必ず大動脈基部圧をモニタし，80 mmHg 以上に保つように確認すること，さらに心筋保護液注入中の大動脈基部を麻酔科医に TEE で描出してもらい，確実に大動脈弁が閉鎖し心筋保護液の注入が行われていることをモニタ画像で確認している．さらに，僧帽弁手術の場合は心筋保護液注入開始後，速やかに左房を切開し，減圧するよう心がけている．

3-3　体外循環の離脱

開胸心膜切開時より心嚢内に CO_2 2～3 L/min を吹き入れて心嚢内に残る空気を少なくするとともに，大動脈遮断解除後の空気抜きは，手術台をさまざまな角度に傾けることでルートカニューレや左房・左室に挿入したベントチューブから行い，麻酔科医により TEE にて残存空気の消失の確認をしてもらい，弁形成などの場合は形成の評価を施行してもらっている．

4 おわりに

当院においては，術前カンファレンスを外科医，心臓外科担当麻酔科医，臨床工学技士，手術室看護師同席の下で行っている．患者の病態については，チームで共通の認識をもって手術に臨むことが必要不可欠であると思われる．

MICSに対応した麻酔法

1 はじめに

MICSは1995年，米国オハイオ州クリーブランドクリニックで始められ，その定義は，①体外循環を用いない，②全胸骨切開を行わない，③その両方，のいずれかの条件を満たすものとされている．疾患別では，体外循環を用いるが全胸骨切開を行わない弁膜症手術や先天性心疾患の手術と，体外循環を用いない心拍動下冠動脈再建術などがある．本稿では，当院で行われている低侵襲法による僧帽弁手術に焦点を当て，その体外循環法と麻酔管理について述べる．

2 麻酔法

MICSの麻酔法は，従来の心臓麻酔と比べ，麻酔薬や循環作動薬の使用について特に大きな違いはなく，心機能や体外循環時間などの条件がそろえば早期抜管を試みる．MICSでは，胸骨非切開ないし小切開を行い，内視鏡支援下に手術を行うため，視野を良くする目的で片肺を虚脱させ，心膜切開や心臓の剥離を行う．このため，ダブルルーメンチューブ，もしくは気管支ブロッカーチューブ(ユニベントチューブなど)を用いて分離肺換気を行うことが要求される．当院では術後に気管内チューブに入れ替える際のリスクを避けるため，気管支ブロッカーチューブを用いている．

3 体外循環前のチェック

心臓血管手術を受ける患者では，動脈硬化病変を有することが多い．術前のCT画像や術中のTEE画像により，大動脈の動脈硬化や石灰化の程度，可動性のプラーク，動脈解離の評価を行い，大動脈のカニューレ挿入部位や遮断部位の変更を行う．上行大動脈の遮断部位は，TEEではblind zoneとなるため，上行大動脈近位部，大動脈弓部，下行大動脈に高度な動脈硬化病変が存在する場合は，上行大動脈に直接超音波探触子を当てる術野エコーで評価を行う．また，周術期にIABP(intra-aortic balloon pump)を留置することもあるが，動脈硬化病変が強い患者では禁忌となる．これらの病変を体外循環前に確認することは，脳塞栓症の予防に重要である[4]．また，左房内血栓，卵円孔開存，左上大静脈遺残など，術前に診断がついていなかった病変や合併奇形を見付けることで，体外循環の様式や術式を変更することもある[5]．

4 送血カニューレと脱血カニューレの挿入

MICSでは，小さな皮膚切開による手術を可能にするため，送血，脱血カニューレを末梢の大血管から挿入し，カテーテル類による術野の混雑を避ける．上行大動脈へのカニュレーションの代わりに大腿動脈に送血カニューレを挿入し，右房からの脱血は大腿静脈から経皮的に脱血カニューレを右房に挿入する．必要に応じて，右内頸静脈からの上大静脈カニューレと，大腿静脈からの下大静脈カニューレによる2本脱血とする．

送血，脱血カニューレの挿入は，TEEで下行大動脈や上・下大静脈を描出して，ガイドワイヤが正しく血管内に存在することを確認したうえで行う．大腿静脈からの脱血カニューレが肝静脈に迷入したり，心房中隔欠損孔や卵円孔開存を介して左房に迷入することがある．また，脱血カニューレがキアリネットワーク*1にぶつかって，下大静脈から右房に進まない場合もある．これらの所見はTEEで確認が可能である．左上大静脈遺残が認められる症例で，bridge veinがない場合や右房を切開する手術の場合は，冠静脈洞への3本目の脱血カニュー

*1 キアリネットワーク
下大静脈の右房への開口部から右心房壁や心房中隔を結ぶ線維状あるいは膜状の構造部で，右房内腫瘍と間違えられることがある．卵円孔開存や心房中隔瘤を合併することが多い．

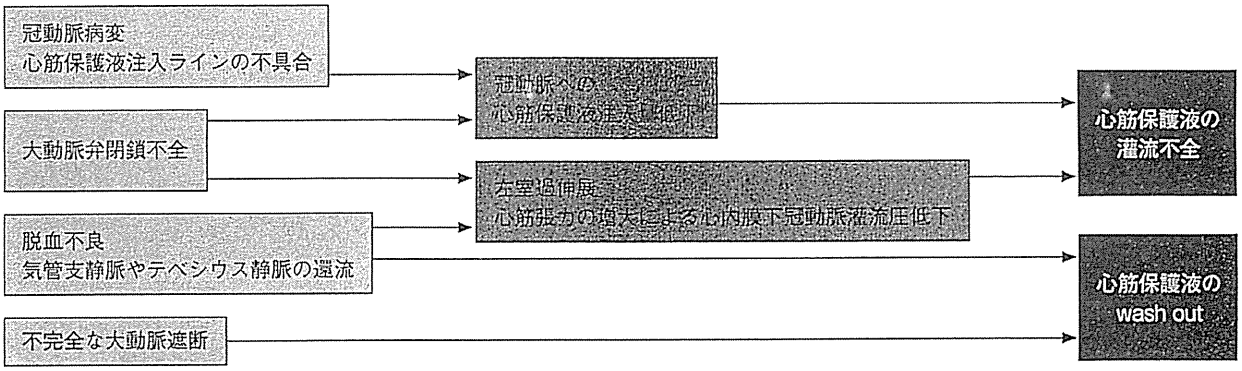

図3　心筋保護が不十分となる機序

レ挿入が必要となる.

5 心筋保護

心筋保護が不十分となる原因は，①心筋保護液の灌流不全と，②心筋保護液の wash out の2つに集約される．具体的には，①大動脈弁閉鎖不全，②冠動脈病変，③心筋保護液注入ラインの不具合，④脱血不良，⑤不完全な大動脈遮断，などがある．大動脈弁閉鎖不全は，冠動脈への心筋保護液の注入量の低下と左室の過伸展により心筋保護液の灌流不全を招く．脱血不良は，左室の過伸展に加え，心筋保護液を wash out してしまう（図3）．これらの異常の早期発見と速やかな対応が重要である．

心筋保護液注入時ならびに心内操作中の左室拡大を予防する目的で，心内ベントを左房，左室，肺動脈などに挿入するが，僧帽弁手術ではベントチューブは心腔内操作後に左室に挿入する．ベントチューブは心腔内遺残空気の除去や，体外循環離脱時に左室機能が十分に回復するまで左室仕事量の低減と左室の過伸展を予防する目的でも用いられる．逆行性冠灌流は，冠動脈高度狭窄病変や大動脈弁疾患で行われるが，左上大静脈遺残が認められる症例では，逆行性冠灌流は無効である．

6 心腔内遺残空気

自己心拍が再開し大動脈遮断が解除された後に，心腔内遺残空気を除去する．心腔内の遺残空気は，ほとんどすべての開心術で認められ，右上肺静脈，右冠動脈洞，左心耳，左室心尖部など心腔内の高いところに貯留しやすい．気泡型と貯留型があり，問題となるのは貯留型である．空気が右冠動脈に迷入して，心電図上 ST 変化や心室の壁運動異常が出現することがあるが，しばらく灌流圧を高めに保つことで回復する．手術台を傾けたり，心臓を揺すったりして，TEE により遺残空気の検索と誘導を行いながら，左房・左室ベントや大動脈基部ベントにより脱気する．開心中の術野での CO_2 使用も空気貯留を減らすうえで有用である．

7 体外循環からの離脱

体外循環からの離脱に際しては，残存逆流はどの程度か，溶血を引き起こす可能性はないか，弁狭窄が起こっていないかなど，手術結果の評価も並行して行う．復温や電解質のチェックを行い，心電図，動脈圧，肺動脈圧，中心静脈圧などの各種モニタで心機能の回復が確認できたら，徐々に心臓に容量負荷をかけ，自己心拍に移行していく．容量負荷により中心静脈圧が大きく上昇し，十分な動脈圧が得られない場合は，いったん脱血して人工心肺による補助循環を行い，心臓の負荷を軽減して，心機能の回復を待つ．体外循環からの離脱が困難な場合は，左室・右室の前負荷，収縮性，壁運動，各弁の機能などを，患者のベースラインと比較することが原因究明の有用な手がかりとなる．

8 まとめ

体外循環の管理を確実に行うことは，安全な手術を保証するうえで重要である．循環モニタ

の中でもTEEは大きな役割を担っており，術式の変更や手術結果の評価だけでなく，合併症の軽減や予後の改善も期待でき，MICSに必須のものとなっている[6),7)]．さらに本手術では，臨床工学技士とのコミュニケーションが必須であり，麻酔科医，心臓外科医，臨床工学技士の連携は手術成績を左右するだけでなく，患者の生命予後にも影響すると考える．

外科医 麻酔科医 臨床工学技士

MICSにおける体外循環法

1 当院における標準的体外循環法

当院での成人体外循環はすべて遠心ポンプ送血，陰圧吸引補助脱血(vaccum assisted venous drainage：VAVD)で行っている[8)]．また，静脈貯血槽バイパス回路があり，体外循環離脱時に静脈貯血槽の流入出口を閉じ，静脈貯血槽バイパス回路を開けることにより閉鎖回路となり，離脱操作を容易にしている．心筋保護装置には「MPS®」(QUEST Medical Inc.)を用いて，患者の心機能の状態に合わせた心筋保護を行っている(図4)．

2 MICSでの体外循環の実際

MICSでの体外循環と従来の心臓手術での体外循環に大きな違いはない．ただし，カニュレーションが末梢血管からとなる．

2-1 体外循環開始

確実なカニュレーションとACT(activated coagulation time)値が480秒を超えたことが確認できたら，体外循環を開始する．MICSでは，体外循環開始後，心膜切開が行われる．このとき適度の脱血により心房を虚脱した状態にする．VAVDでの陰圧の調節はゆっくりと行うことがコツである[9)]．適正灌流量の維持や脱血ができない場合は，脱血カニューレの位置を

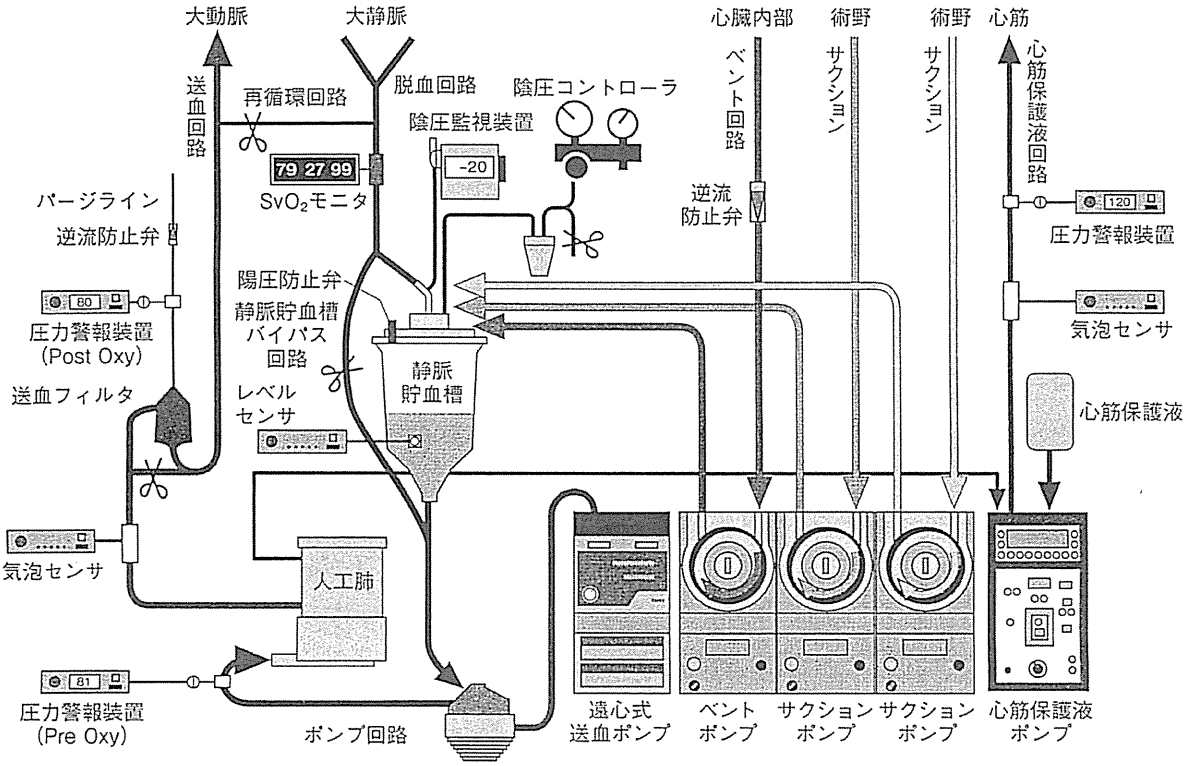

図4 慶應義塾大学病院における人工心肺システム

確認する.

2-2 大動脈遮断，心筋保護液注入

大動脈遮断時は人工心肺の血流量を低下させ，遮断確認後，ゆっくりと血流量を戻す．その後，心筋保護液を注入する．MICSでは切開創から大動脈が深いため，心筋保護液注入カニューレの長さを15 cmから20 cmにし，注入，ベント，圧測定が可能なカニューレを作製した．心筋保護液注入中は注入圧が80～90 mmHgになるように流量を調節する．注入圧が低い場合には，大動脈弁逆流が発生している可能性がある．術野に報告し，TEEで逆流がないか確認する[10]．

2-3 心内操作中の体外循環

心房中隔欠損症例ではVAVDでの陰圧が弱すぎると下大静脈より血液が術野に流入し，無血視野は得られない．強すぎると無血視野は得られるが，脱血回路に大量の気泡が混入し，血液に悪影響を与える．適切な陰圧は，無血視野が得られ，脱血回路への気泡混入が微量な程度の陰圧に調節することである．そのためには術野ビデオモニタ，脱血回路の監視が重要である．一時的に脱血回路に気泡センサを装着し，気泡が検知しない程度に陰圧を調節することも1つの方法である．

僧帽弁症例では，視野を確保するために，左心房吊り上げ鈎(atrialリトラクター)により左心房を牽引する．このとき脱血不良になることがある[11]．その場合，術野に報告し，吊り上げ鈎の位置やカニューレの状態を確認してもらう．また，間欠的な心筋保護液注入時に注入圧が上昇しない場合がある．これは，左心房の牽引により大動脈弁が変形し，逆流が起きるからである[12]．心筋保護液注入時に注入圧が上昇しない場合には，左心房の牽引を一時的に解除し，心筋保護液注入後，再牽引する．

2-4 大動脈遮断解除

心内操作の終了が近付いたら復温を開始する．心内気泡除去のため，左房・左室ベント，大動脈基部ベントができるようにしておく．遮断解除時には血流量を低下させる．解除後，血流量をゆっくりと再開させながら，左房・左室ベント，大動脈基部ベントを開始する．

2-5 体外循環からの離脱

確実な気泡除去が確認されたら，まず左房・左室ベントを抜去する．その後，灌流圧(血圧)が50 mmHg程度になるまで脱血を行い，大動脈基部ベントを抜去する．抜去部分が確実に止血されていることを確認したら，ゆっくりと容量付加を行う．血行動態が安定したら徐々に血流量を下げていき，体外循環から離脱する．

3 MICSにおける体外循環のポイント

MICSにおける体外循環のポイントは，確実なカニュレーションと心筋保護と心内気泡除去である．

3-1 カニュレーション

MICSでの送脱血部位は，良好な視野を確保するために末梢の血管(大腿動脈，大腿静脈，内頸静脈など)が用いられる．そのため，カニューレはPCPSで用いられる経皮用カニューレが使用される．送血部位は大腿動脈である．カニュレーションはカットダウン(direct cutdown insertion)で行われる．ガイドワイヤ挿入時，確実に下行大動脈に挿入されているか，外科医，麻酔科医，臨床工学技士がTEEを観察して確認する．

カニューレは先端に側孔がある「FEM Ⅱ」(エドワーズライフサイエンス(株))を用いている．サイズは，体表面積1.5 m^2以下の症例では16 Fr，1.7 m^2以下では18 Fr，それ以上では20 Frを用いている．血流量が5 L/min以上の症例では，送血を2本に分け，両側の大腿動脈へ18 Frもしくは20 Frのカニューレを挿入して送血を行う．また，大腿動脈が細く16 Frが挿入できない症例では，両側の大腿動脈へ14 Frのカニューレ(小児用)を挿入して送血を行う．図5に両側送血用の回路を示す．

脱血部位は1本脱血では大腿静脈，2本脱血では内頸静脈と大腿静脈である．カニュレーションはdirect cutdown insertionかpercu-

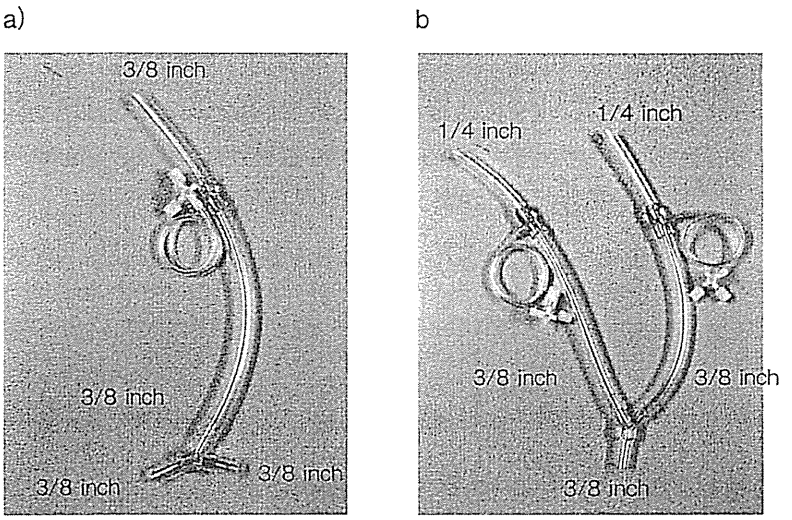

図5　両側送血用回路
a) 血流量 5 L/min 以上の場合.
b) 16 Fr のカニューレが挿入できない場合.

taneous insertion で行われる．どちらの場合もガイドワイヤ，ダイレータを用いてカニュレーションを行う．ガイドワイヤ挿入時，確実に右心房に挿入されているか，外科医，麻酔科医，臨床工学技士が TEE を観察して確認する．また，各サイズのダイレータを用いて確実に皮膚，血管孔を拡張させる．カニューレは側孔が多く，長さが 65 cm ある「VFEM」(エドワーズライフサイエンス(株)) を用いている．サイズは，体表面積 1.5 m^2 以下の症例では 18 Fr，1.6 m^2 以下では 20 Fr，1.7 m^2 以下では 22 Fr，それ以上では 24 Fr を用いているが，良好な脱血状態を維持するために，可能な限り太いカニューレを挿入する．また，脱血カニューレの位置も重要である．特に 1 本脱血の場合，カニューレの先端が上大静脈内まで挿入されなければならない．「VFEM」に附属しているダイレータは 16 Fr までしかないため，18 Fr 以上のカニューレを用いる場合は皮膚，血管孔の拡張が不十分である．そのため，18 Fr，20 Fr，22 Fr，24 Fr のダイレータを用意した．これにより，確実で安全なカニュレーションが可能となった．

3-2　心筋保護

MICS での心筋保護法は，当初，間欠的に順行性に投与する方法が主流であったが，現在では重症例の手術も行うため，順行性や逆行性など患者の状態に合わせた統合的な心筋保護を行っている．また，アイススラッシュなどを用いて局所冷却法を行っても，左心室の冷却は行えない．non-coronary collateral flow により大動脈遮断時でも心腔内に血液が満ち，常温体外循環の場合，心筋が温められてしまう．そのため，心筋保護の目的から体温を 28 ～ 30℃の中等度低体温体外循環を用いる．特に重要なのが注入時にカニューレの先端圧および TEE で逆流などがないか確認することであり，確実な心筋保護を行う．

3-3　心内気泡除去

MICS では，遮断解除後の心臓脱転や用手的な心臓圧迫による心内気泡除去は不可能である．そのため，心膜切開時から心嚢内に 2 ～ 3 L/min の CO_2 を吹送し，心内に残存する空気を少なくするとともに，手術台をいろいろな向きに傾け体位変換しながら，左房・左室ベント，大動脈基部ベントから十分時間をかけて気泡除去を行うことが重要である[13), 14)]．また，血流量を下げ，心臓に容量付加し，肺循環血液量を増加させることにより，肺静脈内の気泡が除去される．最終的に TEE で気泡がないことが確認できるまで，気泡除去を行う．

■文　献

1) Chitwood WR, Elbeery JR, Moran JF, et al: Minimally invasive mitral valve repaire using transthoracic aortic occulusion, Ann Thrac Surg 63(5): 1477-1479, 1997
2) Yozu R, Shin H, Maehara T: Minimally invasive cardiac surgery by the port-access method, Artif Organs 26(5): 430-437, 2002
3) Yozu R, Okamoto K, Kudo M, et al: New innovative instruments facilitate both direct-vision and endoscopic-assisted mini-mitral valve surgery, J Thorac Cardiovasc Surg, in press
4) Wilson MJ, Boyd SY, Lisagor PG, et al: Ascending aortic atheroma assessed intraoperatively by epiaortic and transesophageal echocardiography, Ann Thorac Surg 70(1): 25-30, 2000
5) Practice guidelines for perioperative transesophageal echocardiography. A repot by the American Society of Anesthesiologists and the Society of Cardiovascular Anesthesiologists Task Force on Transesophageal Echocardiography, Anesthesiology 84(4): 986-1006, 1996
6) Fanshawe M, Ellis C, Habib S, et al: A retrospective analysis of the costs and benefits related to alterations in cardiac surgery from routine intraoperative transesophageal echocardiography, Anesth Analg 95(4): 824-827, 2002
7) Practice guidelines for perioperative transesophageal echocardiography. An update report by the American Society of Anesthesiologists and the Society of Cardiovascular Anesthesiologists Task Force on Transesophageal Echocardiography, Anesthesiology 112(5): 1084-1096, 2010
8) 又吉　徹，四津良平，川田志明：低侵襲小切開心臓手術（MICS）とその体外循環の工夫，「体外循環」－落差脱血から吸引脱血へ－，川田志明（編），体外循環と補助循環，日本人工臓器学会セミナー，日本人工臓器学会，p65-76, 1999
9) Toomasian JM, Peters WS, Siegel LC, et al: Extracorporeal circulation for port-access cardiac surjery, Perfusion 12(2): 83-91, 1997
10) Peters WS, Fann JI, Burdon TA, et al: Port-access cardiac surgery: a system analysis, Perfusion 13(4): 253-258, 1998
11) Vanermen H, Vermeulen Y, Wellens F, et al: Port-access mitral valve surgery, Perfusion 13(4): 249-252, 1998
12) Gooris T, Van Vaerenbergh G, Coddens J, et al: Perfusion techniques for port-access surgery, Perfusion 13(4): 243-247, 1998
13) Toomasian JM: Cardiopulmonary bypass for less invasive procedures, Perfusion 14(4): 279-286, 1999
14) Matayoshi T, Yozu R, Morita M, et al: Development of a Completely Closed Circuit Using an Air Filter in a Drainage Circuit for Minimally Invasive Cardiac Surgery, Artificial Organs 24(6): 454-458, 2000

Photochemistry and Photobiology, 2011, 87: 199–207

Photosensitization Reaction-Induced Acute Electrophysiological Cell Response of Rat Myocardial Cells in Short Loading Periods of Talaporfin Sodium or Porfimer Sodium

Arisa Ito*[1], Takehiro Kimura[2], Shunichiro Miyoshi[2], Satoshi Ogawa[3] and Tsunenori Arai[1]

[1]School of Fundamental Science and Technology, Graduate School of Science and Technology, Keio University, Kohoku-ku, Yokohama, Japan
[2]Cardiopulmonary Division, Department of Internal Medicine, Keio University School of Medicine, Shinjuku-ku, Tokyo, Japan
[3]Mita Hospital, International University of Health and Welfare, Minato-ku, Tokyo, Japan

Received 8 August 2010, accepted 20 October 2010, DOI: 10.1111/j.1751-1097.2010.00846.x

ABSTRACT

Electrophysiological responses of rat myocardial cells to exogenous photosensitization reactions for a short period of incubation with two photosensitizers, talaporfin sodium or porfimer sodium, were measured in a subsecond time scale. The loading period of the photosensitizer when the photosensitizer might not be taken up by the cells was selected as 15 min, which was determined by the fluorescence microscopic observation. We measured the intracellular Ca^{2+} concentration ($[Ca^{2+}]_{in}$) by using a fluorescent Ca^{2+} indicator, Fluo-4 AM, under a high-speed confocal laser microscope to evaluate the acute electrophysiological cell response to the photosensitization reaction. The measured temporal change in Fluo-4 fluorescence intensity indicated that the response to the photosensitization reaction might be divided into two phases in both photosensitizers. The first phase is acute response: disappearance of Ca^{2+} oscillation when irradiation starts, which might be caused by ion channel dysfunction. The second phase is slow response: $[Ca^{2+}]_{in}$ elevation indicating influx of Ca^{2+} due to the concentration gradient. The continuous Ca^{2+} influx followed by changes in cell morphology suggested micropore formation on the surface of the cell membrane, resulting in necrotic cell death.

INTRODUCTION

Photosensitization reaction-induced cellular damage has been widely applied to clinical therapies such as noninvasive cancer therapy and age-related macular degeneration (1,2). Photochemical interactions involve photons, photosensitizers and oxygen generate reactive oxygen species, mainly singlet molecular oxygen (3–5). The activated singlet oxygen reacts with many biological molecules, including lipids, proteins and nucleic acids, resulting in apoptotic or necrotic cellular damage (6–8). The cellular response to photosensitization reaction is dependent on photosensitizer distribution, which is determined by the loading process and the physicochemical properties of the photosensitizer molecule, particularly molecular size, structure, charge and water solubility (9,10). The photosensitization reaction may cause selective organelle damage when the photosensitizer localizes to certain cellular compartments such as the mitochondria or lysosomes after a long incubation period (4,6). These damages to organelles may initiate enzyme activation followed by apoptosis. After a short incubation period of several minutes, the photosensitizer may not be taken up into the cells and may be distributed on the cell membrane or outside the cells (5). The membrane-bound photosensitizers irradiated by excitation light may induce membrane disruption, for example, due to micropore formation and ion channel dysfunction, resulting in morphological and electrophysiological changes in the cells (6,11).

Oxidative injury is known to be induced by exposure of cells to exogenous photosensitization reactions that increase intracellular free Ca^{2+} concentrations ($[Ca^{2+}]_{in}$) (12–14). The importance of Ca^{2+} for the viability and electrophysiological function of cells is well recognized (15,16). Ca^{2+} overload may play a role in photosensitization reaction-induced necrotic cell death (6). The intracellular Ca^{2+} dynamics during photosensitization reaction has been studied in various cell types such as erythrocytes (17), cardiomyocytes (18,19) and cancer cells (13,20). However, to our knowledge, there are no reports on the acute effect of exogenous photosensitization reactions on $[Ca^{2+}]_{in}$ in myocardial cells as observed in the subsecond scale.

In this study, we focused on the early events of Ca^{2+} dynamics during the onset of exogenous photosensitization reaction in short period of photosensitizer incubation. The photosensitization reaction was induced by short-time incubation of rat myocardial cells with two distinctive clinically approved photosensitizers, porfimer sodium and talaporfin sodium. Porfimer sodium (Photofrin®), a preparation of hematoporphyrin derivatives (HPD), is the most popular photosensitizer and has been applied to various therapies for malignant tumors (1,21). The lipophilic character of porfimer sodium may cause it to localize in the cell membrane and in the subcellular membrane. The cellular uptake of this photosensitizer has been studied in various types of tumor cells. Its subcellular pharmacokinetics in tumor cells is as follows:

*Corresponding author email: arisa.i@arai.appi.keio.ac.jp (Arisa Ito)

distribution on the cell membrane in the first several tens of minutes of incubation, slow uptake into the cells and then localization to other organelle membranes, especially the mitochondria, lysosome and Golgi apparatus in the final stage (22). The other photosensitizer used was the hydrophilic chlorin photosensitizer talaporfin sodium, also called mono-L-aspartyl chlorin e6 (NPe6), a chlorophyll derivative (1,23). Talaporfin sodium has been approved for early-stage lung cancer therapy in Japan as Laserphyrin® (24,25). Talaporfin sodium has been reported to localize to lysosomes after a long period of incubation (26–28). The change in intracellular Ca^{2+} concentration was measured using a high-speed confocal microscope with a frame rate of five frames per second to assess the electrophysiological cellular responses to photosensitization reactions with talaporfin sodium and porfimer sodium.

MATERIALS AND METHODS

Cell culture. Rat myocardial cells (Primary Cell Co., Ltd., Hokkaido, Japan) were cultured in Medium I (Dulbecco's modified Eagle's medium/nutrient mixture F-12 [D-MEM/F-12] supplemented with 10% fetal bovine serum, 100 U mL^{-1} penicillin and 100 $\mu g\ mL^{-1}$ streptomycin; all from Invitrogen, Carlsbad, CA) in an atmosphere of 95% air and 5% CO_2 at 37°C.

Photosensitizers. The photosensitization reaction was performed using two kinds of photosensitizers, a hydrophilic photosensitizer (talaporfin sodium) and a lipophilic photosensitizer (porfimer sodium). Talaporfin sodium (Meiji Seika Kaisha Ltd., Tokyo, Japan), 799.69 MW, has a major absorption peak of the Q band at 664 nm and an average molar absorbance of $2.7 \times 10^4\ M^{-1}\ cm^{-1}$ at 667 nm in a medium (without phenol red) containing 10% fetal bovine serum (29). Porfimer sodium (Wyeth Lederle, Japan Ltd., Tokyo, Japan), 1,231.28–4,883.30 MW, has a major absorption peak of Q band at 625 nm and an average molar absorbance of $2.9 \times 10^3\ M^{-1}\ cm^{-1}$ at 630 nm in the same mixture as mentioned above (29).

Photocytotoxic effect. The isolated rat myocardial cells were placed in collagen-coated 96 well microplates at a concentration of 2×10^4 cells per well and cultured in Medium I at 37°C in 5% CO_2. After 6–7 days in culture, the cells were loaded with 10–50 $\mu g\ mL^{-1}$ talaporfin sodium or porfimer sodium medium solution and kept in the dark for 30 min. After incubation in the dark, the cells were exposed to a 670 nm red diode laser (OpticalFuel; Sony Co., Ltd., Tokyo, Japan) for talaporfin sodium or 633 nm red diode laser (HPD 5215; Intense Ltd., NJ) for porfimer sodium at a fluence rate of 150 mW cm^{-2} and a total fluence of 1–10 J cm^{-2}. The cell lethality rate with the photosensitization reaction was measured using a water-soluble tetrazolium-8 (WST-8) assay kit (Cell Counting Kit-8; Doujinkagaku Co., Ltd., Kumamoto, Japan). After irradiation, the culture medium was replaced with a medium without the photosensitizer and 10 μL of WST-8 was added to the wells. After 2 h incubation, the absorbance of the reaction products at 450 nm was measured using a microplate absorbance reader (Sunrise™; Tecan Group Ltd., Maennedorf, Switzerland). The cell lethality rate was calculated as a percentage relative to the absorbance of living cells in the reference well without the photosensitization reaction. The absorbance of the complete viable cells (cell lethality rate of 0%) was defined as the difference between the absorbance of the cells with no irradiation without photosensitizer loading and that of the cells irradiated by 10 J cm^{-2} laser light after incubation with 50 $\mu g\ mL^{-1}$ talaporfin sodium or porfimer sodium. The normalized ratios characterized by the above definitions were used to calculate the cell lethality rate.

Subcellular distribution. The isolated rat myocardial cells were grown on 15 mm glass coverslips placed in a 35 mm petri dish 3 days before the experiment. The culture medium was replaced with 30 $\mu g\ mL^{-1}$ talaporfin sodium or porfimer sodium dissolved in Medium II (minimal essential medium supplemented with 10% fetal bovine serum; all from Invitrogen) and then the cells were further incubated for 15 min for 3 h in the dark. To determine the subcellular uptake of the two photosensitizers in rat myocardial cells, the cells incubated with the photosensitizers were stained with a lysosome probe (for talaporfin sodium) or mitochondria probe (for porfimer sodium), since it has been reported that talaporfin sodium localizes to the lysosome and porfimer sodium localizes to the mitochondrion after a long incubation period with tumor cells (10,22,30). After photosensitizer incubation, the cells were washed with the fresh medium without photosensitizer and loaded with a lysosome probe, 1 μM LysoTracker Green (Molecular Probes Inc., Eugene, OR), or mitochondria probe, 1 $\mu g\ mL^{-1}$ Rhodamine 123 (Molecular Probes Inc.) for an additional 30 min at room temperature. After staining, the medium was replaced with a fresh medium and the cells were placed on the stage of an inverted fluorescence microscope (BX51WI; Olympus Co., Ltd., Tokyo, Japan) equipped with ×40 water immersion lens (LUMPlanFL40 × W; Olympus Co., Ltd). Talaporfin sodium or porfimer sodium was excited at 400 ± 10 nm in the Solet band of these photosensitizers, using a 100 W mercury lamp with a band-pass filter, and the fluorescence was detected with a 600 nm long-pass filter. LysoTracker Green or Rhodamine 123 was excited by green light with a 470–495 nm band-pass filter, whereas a 510–550 nm band-pass filter was used to detect fluorescence. No interference was observed between the photosensitizers and organelle probe in the wavelengths used. Fluorescence images for both photosensitizers were taken using a near-infrared cooled CCD camera (Rolera-XR; QImaging, Burnaby, Canada). Image analysis was performed using ImageJ 1.41 (National Institute of Health, Bethesda, MD).

Intracellular Ca^{2+} concentration during the photosensitization reaction. Myocardial cells were grown on 15 mm glass coverslips placed in a 35 mm Petri dish for 2 days and then the change in intracellular free Ca^{2+} concentration ($[Ca^{2+}]_{in}$) during the exogenous photosensitization reaction was examined using a fluorescent Ca^{2+} indicator, Fluo-4 AM (Molecular Probes Inc). Fluo-4, a type of Fluo-4 AM hydrolyzed by cellular esterases inside the cells, has an absorption peak at 494 nm and a fluorescence peak at 516 nm (31,32); thus, the measurement of Fluo-4 fluorescence will not affect the photosensitization reaction. To measure the cellular response to the exogenous photosensitization reaction, in $[Ca^{2+}]_{in}$, the cells were loaded with 5 μM Fluo-4 AM dissolved in Medium II to a 2.2 mM total Ca^{2+} concentration in the medium for 20 min at room temperature. The medium was then replaced with 30 $\mu g\ mL^{-1}$ talaporfin sodium or porfimer sodium for an additional 15 min. In this loading condition of "short period of incubation," both talaporfin sodium and porfimer sodium may not be taken up into the cells. The reaction was observed under a fluorescence microscope to determine the subcellular photosensitizer localization. The amount of photosensitizer taken up into the cellular compartment in the 15 min loading period might be less than 1/10 of that in 30 min incubation for talaporfin sodium. Porfimer sodium has been reported to distribute on the cell membrane in less than 2 h of incubation (22). The cell response in the condition of "long period of photosensitizer incubation" was also measured to compare the cellular response between the loading periods of photosensitizer. A long loading period was determined to be 1 h for talaporfin sodium and 3 h for porfimer sodium. Figure 1 shows the experimental setup for the measurement of $[Ca^{2+}]_{in}$ in rat myocardial cells during the photosensitization reaction with talaporfin sodium or porfimer sodium. Fluo-4 in the myocardial cells was excited with an argon laser at 488 nm (800BL; National Laser Co., Salt Lake City, UT) and talaporfin sodium or porfimer sodium was excited at 655 ± 25 nm (103 mW cm^{-2}) or 625 ± 25 nm (117 mW cm^{-2}), respectively, using a 100 W mercury lamp with a band-pass filter. Fluo-4 fluorescence images were obtained with a confocal laser microscope system (CSU-X1; Yokogawa Electric Company, Tokyo, Japan) mounted on a differential interference microscope (BX51WI-FL-IRDIC; Olympus Co., Ltd) with ×40 water immersion lens. Fluo-4 fluorescence was detected at the 500–540 nm band-pass filter with an electron multiplication CCD camera (DU897; Andor Technology, Belfast, UK) with a frame rate of 200 ms per frame. The detected images were analyzed by the image software iQ Core (Andor Technology). The average Fluo-4 fluorescence intensity inside the cells was used to assess the changes in $[Ca^{2+}]_{in}$ in myocardial cells.

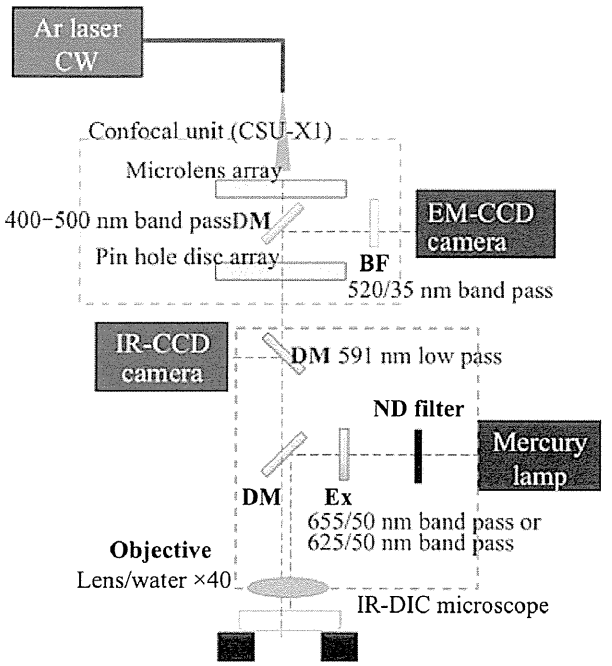

Figure 1. Experimental setup for the measurement of intracellular Ca^{2+} concentration in rat myocardial cells, using a high-speed confocal laser microscope during the photosensitization reaction with talaporfin sodium or porfimer sodium.

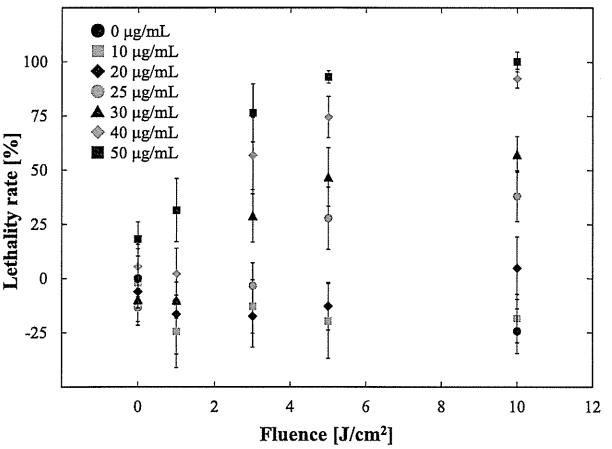

Figure 2. Cell lethality rate in the photosensitization reaction with talaporfin sodium was dependent on the fluence and photosensitizer concentration at the loading time of 30 min.

RESULTS

Photocytotoxic effect of photosensitization reaction with talaporfin sodium or porfimer sodium in rat myocardial cells

The examined parameters in the photosensitization reaction were photosensitizer concentration, laser light energy (in fluence, J cm^{-2}) and loading period. The variation in loading period induced little difference in photocytotoxicity. Figures 2 and 3 show the cell lethality change with fluence in various photosensitizer concentrations at the loading time of 30 min.

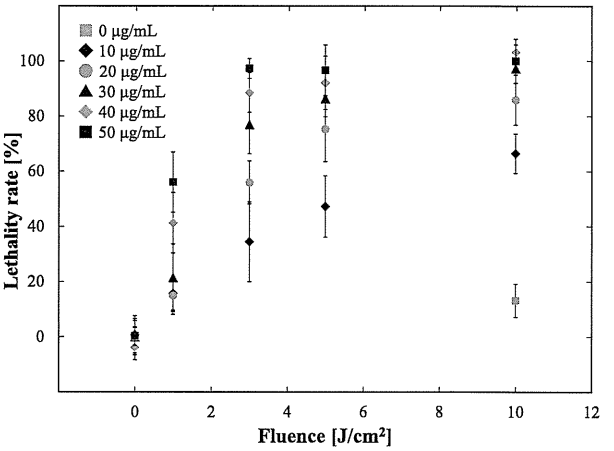

Figure 3. Cell lethality rate in the photosensitization reaction with porfimer sodium was dependent on the fluence and photosensitizer concentration at the loading time of 30 min.

The same tendency was observed in both photosensitizers; that is, the lethality rate increased with the increase in photosensitizer concentration and fluence. When the lethality rate was more than 50%, drastic morphological changes in cells were observed from the phase-contrast microscopic observation: first, a granulated cytoplasm, then bleb formation and finally cell shrinkage were seen. The photosensitizer concentration was selected as 30 μg mL^{-1} for the subsequent study based on the following requirements: more than 50% lethality rate at 10 J cm^{-2} and monotonous increase in lethality up to 10 J cm^{-2}.

Subcellular distribution of talaporfin sodium or porfimer sodium in rat myocardial cells

The subcellular distribution of talaporfin sodium and porfimer sodium in rat myocardial cells with the short loading period of up to 1 h in talaporfin sodium and 3 h in porfimer sodium was determined using a fluorescence microscope. The bright-field image, talaporfin sodium fluorescence image, LysoTracker Green fluorescence image and the merged image of talaporfin sodium fluorescence (red) and LysoTracker Green fluorescence (green) using the same myocardial cells at the incubation times of 15 min, 30 min and 45 min are shown in Fig. 4a–l. In the fluorescence image of Fig. 4b, the narrow distribution of talaporfin sodium, unlike the LysoTracker fluorescence distribution (Fig. 4d), indicates that talaporfin sodium might not be taken up into the cells in the 15 min loading period. When cells were incubated with talaporfin sodium for 30–45 min, the photosensitizer fluorescence distribution corresponded with the LysoTracker Green fluorescence distribution (Fig. 4h,l), which indicates that talaporfin sodium was taken up into the myocardial cells and localized to the lysosome over the 30 min incubation time.

The bright-field image, porfimer sodium fluorescence image, Rhodamine 123 fluorescence image and the merged image of porfimer sodium fluorescence (red) and Rhodamine 123 fluorescence (green) using the same myocardial cells in incubation times of 30 min, 2 h and 3 h are shown in Fig. 5a–l. In the case of 30 min incubation (Fig. 5b), the

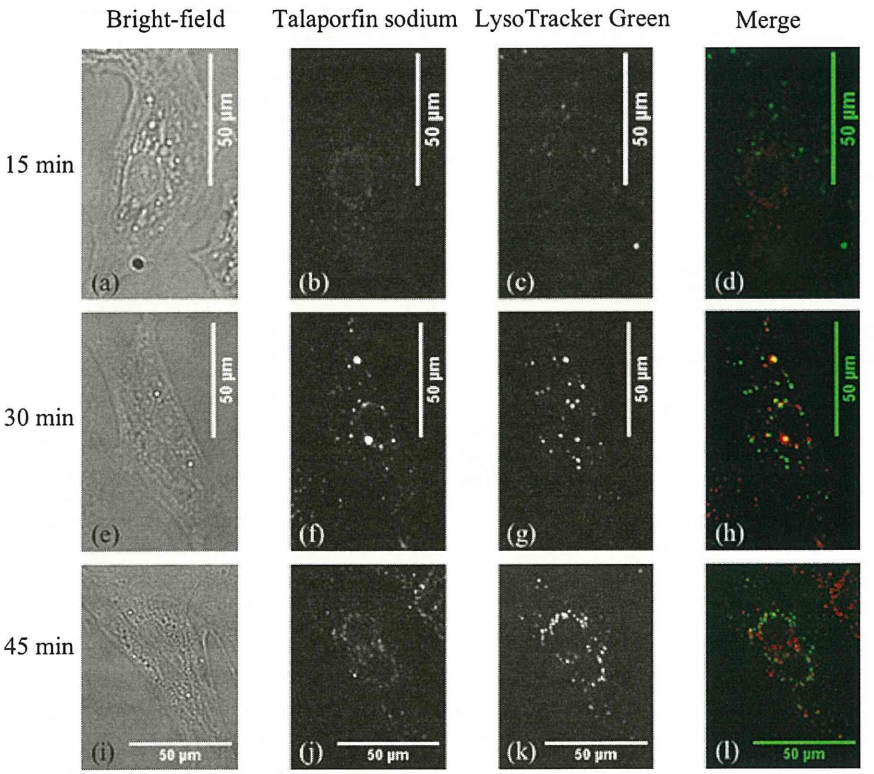

Figure 4. Intracellular talaporfin sodium distribution in rat myocardial cells. The cells were incubated in the medium containing talaporfin sodium (30 μg mL^{-1}) for 15 min [(a)–(d)], 30 min [(e)–(h)] and 45 min [(i)–(l)]. From left to right, bright-field image, talaporfin sodium fluorescence image, LysoTracker Green fluorescence image and the merged image of talaporfin sodium fluorescence and LysoTracker Green fluorescence.

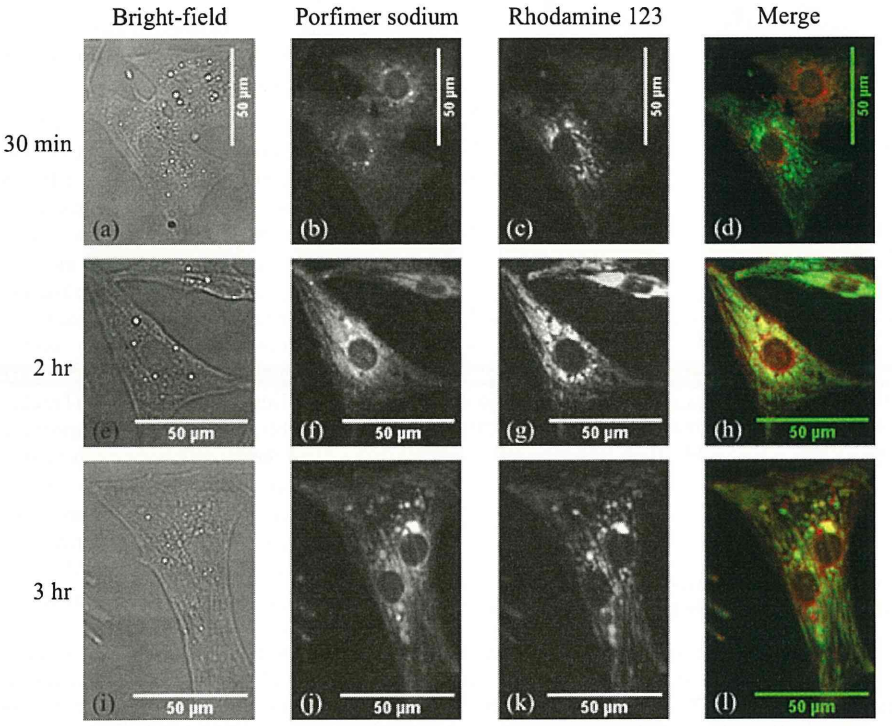

Figure 5. Intracellular porfimer sodium distribution in rat myocardial cells. Cells were incubated in the medium containing porfimer sodium (30 μg mL^{-1}) for 30 min [(a)–(d)], 2 h [(e)–(h)] and 3 h [(i)–(l)]. From left to right, bright-field image, porfimer sodium fluorescence image, Rhodamine 123 fluorescence image and the merged image of porfimer sodium fluorescence and Rhodamine 123 fluorescence.

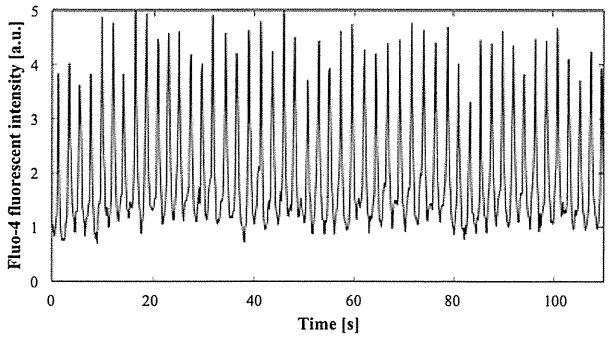

Figure 6. Changes in the control Fluo-4 fluorescence intensity without irradiation and with talaporfin sodium at 15 min loading.

almost uniform dim light of porfimer sodium fluorescence in all cells indicates that porfimer sodium was distributed in the cell membrane. The similarity between the fluorescence images of porfimer sodium and Rhodamine 123 was observed over 2–3 h of incubation (Fig. 5h,l). These results indicate that porfimer sodium distributed on the cell membrane at first for several tens of minutes of incubation and then relocalized to the mitochondria after several hours of further incubation.

Intracellular Ca^{2+} concentrations during the photosensitization reaction with talaporfin sodium or porfimer sodium

The acute subsecond response of intracellular free Ca^{2+} concentration ($[Ca^{2+}]_{in}$) of the myocardial cells to the exogenous photosensitization reaction with talaporfin sodium or porfimer sodium for a short period of photosensitizer incubation (15 min) was measured by using a confocal laser microscope. The time courses of the change in normal Fluo-4 fluorescence intensity in single myocardial cells are shown in Fig. 6, with the control condition being the presence of photosensitizer and the absence of photoactivation. The change in normal Fluo-4 fluorescence intensity of single myocardial cells was obtained as a control during the measurement period of 110 s. The well-known periodic change in intracellular Ca^{2+} concentration accompanied by excitation and contraction processes of myocardial cells, the so-called Ca^{2+} oscillation, was observed as the periodic increase and decrease in Fluo-4 fluorescence intensity (data not shown). The periodic change in Fluo-4 fluorescence intensity was not influenced by the addition of talaporfin sodium to the control (Fig. 6); the same result was obtained with porfimer sodium. There was almost no Fluo-4 photobleaching in this experimental setting during the measurement period. The laser used for Fluo-4 excitation was found to have less influence on the measurement of Fluo-4 fluorescence during the photosensitization reaction.

Figure 7a,b shows the change in Fluo-4 fluorescence intensity in single myocardial cells during the exogenous photosensitization reaction after the short period of incubation with talaporfin sodium (Fig. 7a) and porfimer sodium (Fig. 7b). A similar temporal pattern in the recorded change in Fluo-4 fluorescence intensity between both photosensitizers was observed when the photosensitizer was mainly located outside the cells. Soon after the start of irradiation, the amplitude of the periodic oscillation in the Fluo-4 fluorescence intensity

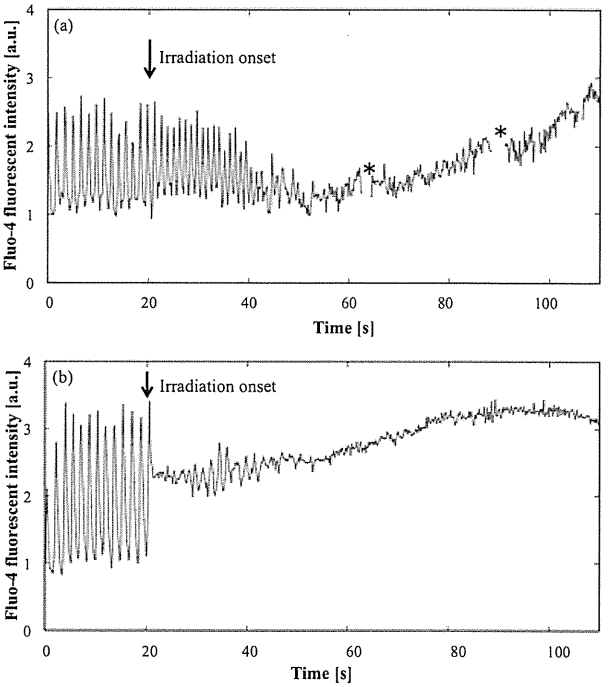

Figure 7. Changes in Fluo-4 fluorescence intensity during the exogenous photosensitization reaction after a short period of incubation with (a) talaporfin sodium and (b) porfimer sodium. The asterisks shown in the graph indicate the break for the focus adjustment.

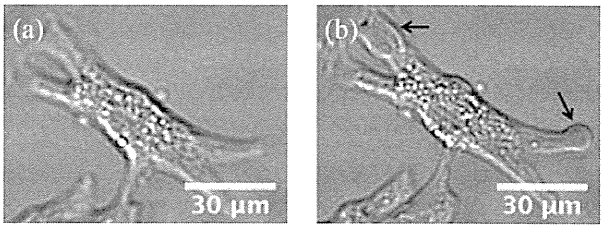

Figure 8. Morphological change (a) before and (b) 5 min after the photosensitization reaction with talaporfin sodium in a certain cell. The arrows shown in (b) indicate bleb formation.

disappeared within a few seconds. A subsequent irradiation induced a gradual increase in $[Ca^{2+}]_{in}$, which eventually exceed the maximum value in the normal oscillation. A drastic morphology change after the photosensitization reaction for the short period of incubation with talaporfin sodium, such as bleb formation, was observed on the surface of the myocardial cells without visible damage to the nuclei (Fig. 8), which was also observed in the reaction with porfimer sodium. However, there were differences in the extent of temporal response of the Fluo-4 fluorescence intensity to the photosensitization reaction between the photosensitizers. The time required for the oscillation amplitude to disappear was longer in the reaction with talaporfin sodium than that with porfimer sodium. A gentle slope in the temporal Fluo-4 fluorescence intensity change was obtained with talaporfin sodium.

In contrast, the photosensitization reaction with the photosensitizers distributed in the intracellular compartment showed a difference in the temporal tendency of the electrophysiological

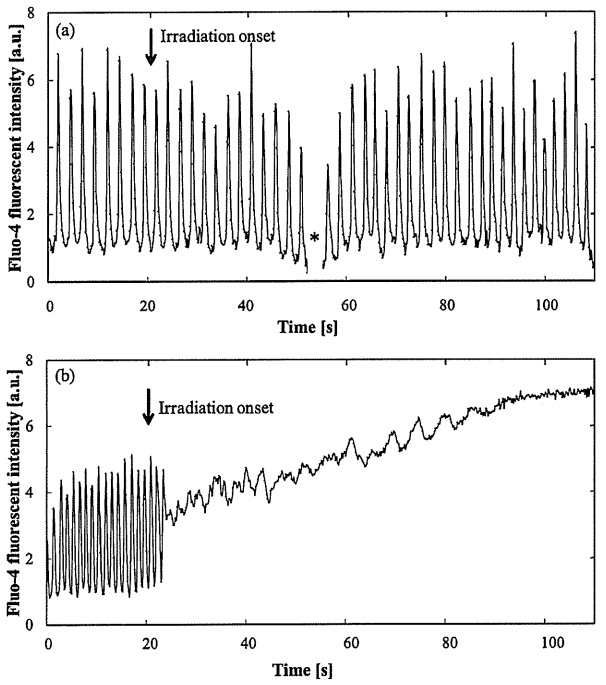

Figure 9. Changes in Fluo-4 fluorescence intensity during photosensitization reaction after a long period of incubation with (a) talaporfin sodium and (b) porfimer sodium. The asterisks shown in the graph indicate the break for the focus adjustment.

response between talaporfin sodium and porfimer sodium (Fig. 9a,b). Little change in the periodic oscillation of fluorescence intensity was observed with the photosensitization reaction in the long period of incubation with talaporfin sodium (Fig. 9a), indicating that the damage in the intracellular compartment, especially in lysosomes, might cause almost no acute effect on the electrophysiological cellular function. On the other hand, the photosensitization reaction in the long period of incubation with porfimer sodium induced the same response as in the short period of the photosensitizer incubation (Fig. 9b).

DISCUSSION

The subsecond intracellular calcium responses of rat myocardial cells to the photosensitization reaction for a short period of photosensitizer incubation showed similar temporal tendencies between both photosensitizers, talaporfin sodium and porfimer sodium (Fig. 7). The temporal characteristics of the Fluo-4 fluorescence intensity triggered by the photosensitization reaction could be divided into two phases: the first phase was the disappearance of Ca^{2+} oscillation, called the "phase I acute response," and the second phase was the gradual increase in $[Ca^{2+}]_{in}$, called the "phase II slow response." The regular spike showing normal activity of myocardial cells obtained before irradiation disappeared within the first several tens of seconds after the onset of photoactivation. This acute response might be caused by ion channel dysfunction because no microscopically significant cell morphological change was observed. After the disappearance of automaticity, there was a brief period of relatively constant level of Fluo-4 fluorescence

Table 1. The experimentally obtained decay time of the Ca^{2+} oscillation amplitude and average rate of change in $[Ca^{2+}]_{in}$ in various conditions.

	Talaporfin sodium		Porfimer sodium	
	Short period incubation	Long period incubation	Short period incubation	Long period incubation
Decay time of the Ca^{2+} oscillation amplitude (s)	11	-*	9.9	6.8
Average rate of change in $[Ca^{2+}]_{in}$ (nM s^{-1})	20.1	-*	44.5	82.9

*In the condition of long period of incubation with talaporfin sodium, there was almost no cellular response in $[Ca^{2+}]_{in}$ to the photosensitization reaction during the measurement period up to 200 s, so that the decay time and the average rate of $[Ca^{2+}]_{in}$ change defined as above definitions is not calculated.

intensity, followed by a gradual increase in Fluo-4 fluorescence intensity as the phase II slow response occurs. The elevation of the Fluo-4 fluorescence intensity in phase II is possibly induced by the Ca^{2+} influx due to the difference in Ca^{2+} concentration between inside and outside the cell. The Ca^{2+} influx and cell morphological changes such as bleb formation indicate that the photosensitization reaction in the short period of incubation might cause cell membrane damage, mostly micropore formation on the surface of the cell membrane.

To compare the early electrophysiological cellular response to the photosensitization reaction between the photosensitizers and between their distributions, the temporal characteristic of the change in intracellular Ca^{2+} concentration with the photosensitization reaction was examined in both the phase I acute response and the phase II slow response. We focused on one parameter in each phase. The first one in the phase I acute response is "decay time of the Ca^{2+} oscillation amplitude," which is defined as the time required for the oscillation amplitude in the Fluo-4 fluorescence intensity to decrease to 1/e of the pre-irradiation average value after the onset of the irradiation. The oscillation amplitude in the fluorescence intensity was defined as the difference between the maximum and minimum fluorescence intensities during the oscillation period obtained before the onset of irradiation. The oscillation amplitude decreased with time during the photosensitization reaction. The decay times of the oscillation amplitude in the three conditions, talaporfin sodium with a short period of incubation and porfimer sodium with a short/long period of incubation, are shown in Table 1. The decay time was longer in the photosensitization reaction with talaporfin sodium than that with porfimer sodium.

The second parameter is "average rate of change in $[Ca^{2+}]_{in}$" in the phase II slow response. After the oscillation disappearance followed by a brief period of relatively constant level in $[Ca^{2+}]_{in}$, then $[Ca^{2+}]_{in}$ began to increase with time. We define "average rate of change in $[Ca^{2+}]_{in}$" during about 20 s after the initiation of the $[Ca^{2+}]_{in}$ increase. To obtain the average rate of change in $[Ca^{2+}]_{in}$, the estimated intracellular Ca^{2+} concentration was calculated from the measured Fluo-4 fluorescence intensity in the range of the normal oscillation amplitude using the following equation (33).

$$[Ca^{2+}]_{in} = K_d \frac{F - F_{min}}{F_{max} - F} \quad (1)$$

where K_d is the dissociation constant of Fluo-4 reported to be 345 nM (32,34), F_{min} is the Fluo-4 fluorescence intensity in the absence of Ca^{2+}, F_{max} is the fluorescence intensity in saturated Ca^{2+} and F is the fluorescence intensity in intermediate Ca^{2+} levels. We assume that F_{min} is zero to calculate the intracellular Ca^{2+} concentration from Eq (1). The fluorescence intensity is normalized by the minimum value of the oscillation intensity before the irradiation onset, where $[Ca^{2+}]_{in}$ is assumed to be 100 nM (35). The average rate of change in $[Ca^{2+}]_{in}$ was obtained from the changes in $[Ca^{2+}]_{in}$ during the photosensitization reaction calculated using Eq (1). We assume that these gradual increases in $[Ca^{2+}]_{in}$ several tens of seconds after the initiation of $[Ca^{2+}]_{in}$ increase might be caused by the micropores formed on the cell membrane in the early stage of the photosensitization reaction and then by the Ca^{2+} influx through the micropores (13). The amount of the photosensitizer and oxygen might be restricted by the limited volume of our experimental setup; thus, oxygen might be possibly exhausted during the early stage of the photosensitization reaction. The initial oxygen concentration in the medium might correspond to 220 μM in the air-saturated solution at 25°C. The oxygen concentration of the photosensitizer solution might have suddenly decreased at the onset of the photosensitization reaction. Several observation of the exhaustion of oxygen during photosensitization reaction has been reported. For example, our research group has reported that oxygen concentration was decreased to 40% of the initial value after the photosensitization reaction with 6.0 μg mL^{-1} talaporfin sodium solution in the condition when the fluence was 1 J cm^{-2} and fluence rate was 200 mW cm^{-2} with a red diode laser (CW, λ = 670 nm) (29). We assume that a certain number of micropores might be formed in the photosensitization reaction with a limited amount of O_2 and then Ca^{2+} influx through the micropores might occur due to the difference in intracellular and extracellular Ca^{2+} concentrations. Table 1 shows the experimentally obtained average rate of change in $[Ca^{2+}]_{in}$ in three conditions: in the short period of incubation with talaporfin sodium and in the short/long period of incubation with porfimer sodium. The photosensitization reaction in the short period of incubation with porfimer sodium is found to induce twice as high average rate of change in $[Ca^{2+}]_{in}$ as with talaporfin sodium.

The shorter decay time of the Ca^{2+} oscillation amplitude (Table 1) and the higher average rate of change in $[Ca^{2+}]_{in}$ (Table 1) were obtained in the photosensitization reaction with porfimer sodium. We think that the parameter in phase I acute response, decay time of the Ca^{2+} oscillation amplitude, indicate the extent of the damage in cellular electrophysiological function such as ion channel malfunction and the other parameter in phase II slow response, average rate of change in $[Ca^{2+}]_{in}$, indicate the extent of the damage in cell membrane such as micropore formation. The results (Table 1) indicate that the earlier cellular response to the photosensitization reaction and the higher efficiency in membrane damage might be obtained with porfimer sodium than with talaporfin sodium. In our experimental condition, the molar energy of absorption per unit volume per unit time was higher with talaporfin sodium (2.8×10^3 J s^{-1} M^{-1} cm^{-3}) than with porfimer sodium (3.4×10^2 J s^{-1} M^{-1} cm^{-3}). Talaporfin sodium has been reported to have a larger triplet quantum yield than porfimer sodium (36), while the triplet state quenching rate is almost the same between the two photosensitizers: 1.3×10^9 M^{-1} s^{-1} for talaporfin sodium (37) and $1.4–1.8 \times 10^9$ M^{-1} s^{-1} for porfimer sodium (38–40). The singlet oxygen quantum yield in talaporfin sodium, 0.77 (37), is larger than that in HPD, 0.06–0.63 (38,41). Despite the higher singlet oxygen quantum yield and the higher molar energy of absorption in the photosensitization reaction with talaporfin sodium, our experimental results indicate that the slower response rate and lower efficiency in micropore formation might be affected by another factor, which might be the photosensitizer location. The photocytotoxic process depends on the distance between the photosensitizer and target cell or subcellular compartment due to the short diffusion path of the singlet oxygen during the lifetime (< 4 μs) in aqueous medium (42). In our experimental condition of short or long period of incubation with porfimer sodium, the lipophilic porfimer sodium might be located on and/or inside the cell membrane (Fig. 5). Lipophilic porphyrins have been reported to generate $^1O_2$ within the membrane bilayer in photoactivation, which might cause membrane protein damage, resulting in electric depolarization, increased permeability, membrane rupture and cell lysis (43–45). The intrinsic lifetime of $^1O_2$ has been reported to be relatively long (13–35 μs) in the lipid bilayer (46,47). Moreover, the membrane-bound porfimer sodium might cause lipid peroxidation effectively in type I reactions (48). In our experimental condition of long period of incubation, a large number of porfimer sodium molecules might be located between the lipid bilayer; thus, the porfimer sodium binding to cell membrane bilayer could induce a more effective micropore formation than that in the short period of incubation. On the other hand, the hydrophilic talaporfin sodium could not bind to the cell membrane; thus, its distance from the cell membrane might be longer than that of porfimer sodium. The singlet oxygen generated from the photoactivation of talaporfin sodium might interact with the cell membrane within an activation length. The activation length might be a diffusion radius of singlet oxygen during the lifetime, reported to be < 220 nm in aqueous solution (49). In our experimental condition for a short period of incubation with talaporfin sodium, the generated singlet oxygen, which might exist within the activation distance from the cell membrane, could cause micropore formation. Despite the long distance from the cell membrane, the higher amounts of singlet oxygen generated in the photosensitization reaction with talaporfin sodium might cause the same level of photocytotoxicity as with porfimer sodium. No electrical responses were observed in the condition of long period of incubation (Fig. 9a). Since talaporfin sodium was localized to the subcellular compartment, especially in the lysosome (Fig. 4), the singlet oxygen might be generated inside the lysosome. The activation path length of the singlet oxygen in the cell has been reported to be 10–20 nm (50,51). The singlet oxygen generated inside the lysosome might cause focal damage of the lysosome, resulting to apoptotic cell death.

In this study, we found that exogenous photosensitization reactions for a short period of photosensitizer incubation induce acute electrophysiological cellular responses and cell membrane damage with similar temporal tendencies between two photosensitizers; talaporfin sodium and porfimer sodium.